Manipulating Magnetic Plasmon Propagation in Metallic Nanocluster Networks

ARTICLE *in* ACS NANO · MAY 2012

Impact Factor: 12.88 · DOI: 10.1021/nn301393x · Source: PubMed

7 AUTHORS, INCLUDING:

Shaunak Mukherjee
Applied Materials
10 PUBLICATIONS **757** CITATIONS
SEE PROFILE

Yang li
Xiamen University
24 PUBLICATIONS **172** CITATIONS
SEE PROFILE

Lisa V Brown
Rice University
10 PUBLICATIONS **891** CITATIONS
SEE PROFILE

Naomi J Halas
Rice University
329 PUBLICATIONS **35,584** CITATIONS
SEE PROFILE

Manipulating Magnetic Plasmon Propagation in Metallic Nanocluster Networks

Na Liu,[†,#,*] Shaunak Mukherjee,[‡,#] Kui Bao,[§,#] Yang Li,[§] Lisa V. Brown,[‡] Peter Nordlander,[†,§,⊥] and Naomi J. Halas[†,‡,§,⊥,*]

[†]Department of Electrical and Computer Engineering, [‡]Department of Chemistry, [§]Department of Physics and Astronomy, and [⊥]Laboratory for Nanophotonics, Rice University, 6100 Main Street, Houston, Texas 77005, United States. [#]These authors contributed equally to this work.

ABSTRACT

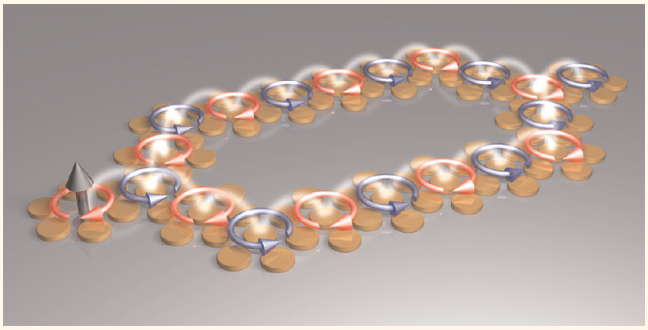

Neighboring fused heptamers can support magnetic plasmons due to the generation of antiphase ring currents in the metallic nanoclusters. In this paper, we use such artificial plasmonic molecules as basic elements to construct low-loss plasmonic waveguides and devices. These magnetic plasmon-based complexes exhibit waveguiding functionalities including plasmon steering over large-angle bends, splitting at intersections, and Mach–Zehnder interference between consecutive Y-splitters. Our findings provide a strategy for circumventing significant challenges in the miniaturization and high-density integration of optical circuits in integrated optics, allowing for the development of ultracompact plasmonic networks for practical applications.

KEYWORDS: magnetic plasmons · nanoclusters · coupling · subwavelength · waveguides · networks

Plasmons of metallic nanostructures, despite being described by classical electromagnetic theory, exhibit characteristics analogous to the wave functions of atoms and molecules.[1] One of the simplest examples of this analogy is a dimer composed of two gold nanoparticles. When the two particles are brought into close proximity, their plasmons mix and hybridize, giving rise to the formation of bonding and antibonding plasmonic modes.[2] This interaction closely resembles the formation of molecular orbitals in a homonuclear diatomic molecule. Plasmon hybridization theory can also be used to analyze the modes of multicomponent plasmonic nanoclusters with more complex geometries.[3,4] For instance, a plasmonic heptamer, with the D_{6h} symmetry of a benzene molecule, has been shown to possess an intriguing Fano resonance due to the interference of its hybridized subradiant and super-radiant modes.[5−9]

Plasmonic circuitry based on metallic nanostructures is a promising potential component of semiconductor-based large-scale integrated circuits.[10−12] Optical frequency signals can be coupled to and propagated along plasmonic structures, which are not subject to the free-space diffraction limit of light.[10] Maier *et al*. demonstrated that an electric plasmon waveguide composed of gold nanoparticles in a linear chain can support subwavelength electric plasmon propagation.[13,14] However, due to significant losses, electric plasmon propagation along such a chain is restricted to a few hundred nanometers at best. Recently, we have shown that magnetic plasmons can efficiently propagate along a conjugated heptamer chain with a much larger field decay length of several micrometers,[15] providing a practical strategy for plasmon-based signal propagation.

In this article we investigate the optical properties of two complex nanoparticle nanoclusters whose spatial geometries are analogues of the organic molecules chrysene and triphenylene.[16] We demonstrate that these artificial plasmonic molecules can serve as building blocks for magnetic waveguiding networks with a variety of functionalities. We first present a plasmon steerer based on an artificial chrysene molecule (Figure 1a), which can direct magnetic plasmons around large-angle bends. We then discuss a plasmon Y-splitter based on an artificial triphenylene molecule

* Address correspondence to nl7@rice.edu, halas@rice.edu.

Received for review March 29, 2012 and accepted May 2, 2012.

Published online May 02, 2012
10.1021/nn301393x

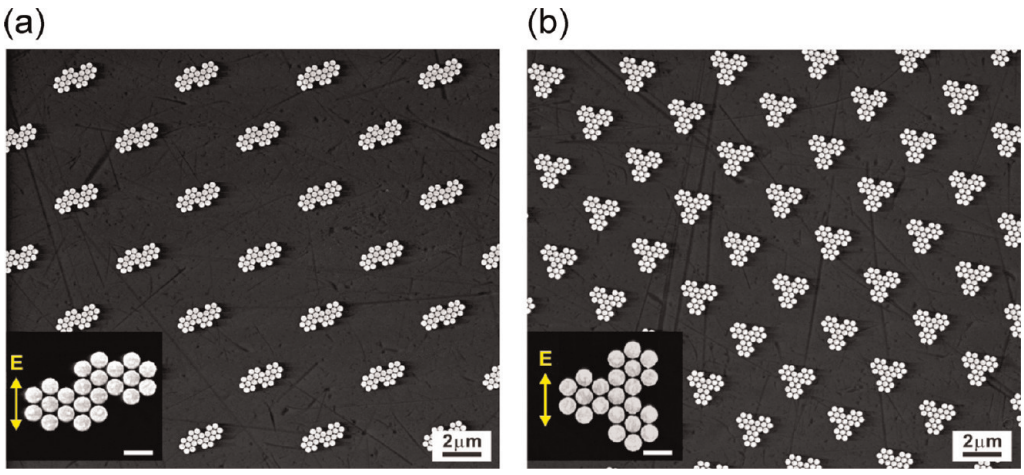

Figure 1. ESEM images of an array of plasmonic chrysene structures (a) and plasmonic triphenylene structures (b) fabricated by electron-beam lithography. Insets: Enlarged views of individual structures with scale bars of 500 nm. The incident light polarization for spectral measurements is indicated in the insets.

(Figure 1b), which can transport magnetic plasmons along two separate optical paths. Both of these magnetic plasmon waveguides exhibit propagation lengths of more than two micrometers, showing superior performance compared to their electric plasmon counterparts. We further show that a plasmon Y-splitter can also serve as an interferometric device to switch magnetic plasmon propagation on and off. Depending on the number of heptamer units on each branch of the splitter, constructive or destructive interference of the magnetic plasmons can take place between the two optical paths. Finally, we present a Mach–Zehnder interferometer composed of two consecutive Y-splitters, which can efficiently split and combine propagating magnetic plasmons. Our magnetic plasmon-based subwavelength waveguides will provide an important blueprint for designing a new generation of nanoscale photonic devices with potential applications in energy transport, data storage, near-field microscopy, and other nanometer-scale technologies.[17–22]

RESULTS AND DISCUSSION

Figure 1a and b present scanning electron microscopy images (ESEM, FEI Quanta 400) of the plasmonic chrysene and triphenylene structures, respectively. The structures were fabricated by electron-beam lithography on a quartz substrate using a positive resist (polymethyl methacrylate, PMMA). After development, a 2 nm chromium adhesion layer followed by an 80 nm layer of gold was evaporated onto the structures by electron-beam evaporation. Subsequently, the PMMA was removed by lift-off in *N*-methyl-2-pyrrolidone. Each sample consists of an array of structures covering an area of 80 μm $\times$ 80 μm. The periodicities in both directions for each structure are 2600 nm. The diameter and thickness of the gold particles are 260 and 80 nm, respectively, and the interparticle gap distance is 30 nm (Figure 1). The spacing between the unit cells does not lead to diffractive coupling in our spectral region of interest.

The optical properties of the samples were characterized using a Fourier-transform infrared spectrometer (FTIR, Bruker Vertex 80v) equipped with a microscope (Hyperion 3000). For excitation of the structures, we utilized linearly polarized light at normal incidence. The direction of polarization is indicated by the yellow arrows in the insets of Figure 1. The measured extinction (1-transmittance) spectrum of the plasmonic chrysene structure is shown in Figure 2a. There are two subradiant resonances that appear as minima at 1100 and 1500 nm within the broad spectral profile of the structure. In order to identify the spectral characteristics, simulations were performed using a commercial implementation of the finite element method (COMSOL Multiphysics). In the simulations, a single nanostructure was defined in the simulation window, and the extinction and absorption fields were solved. Perfectly matched layer and scattering boundary conditions were used to eliminate numerical artifacts at the simulation window boundary. The permittivity of the glass substrate was taken as 2.1, and the empirical dielectric function of bulk gold (Johnson and Christy) was used.[23] The chromium layer was not included in the simulations because it only slightly weakens the spectral response and does not change the underlying physics. The experimental spectrum shows good qualitative agreement with the simulated spectrum. Differences are likely due to inhomogeneous broadening in the ensemble measurement caused by fabrication tolerances. Nevertheless, all of the main spectral features including the two distinct resonance dips are clearly observed in the experiment.

To further investigate the underlying physics, electromagnetic field plots were generated at 1100 and 1500 nm. The shorter wavelength at 1100 nm is associated with a multiple Fano resonance mode, in

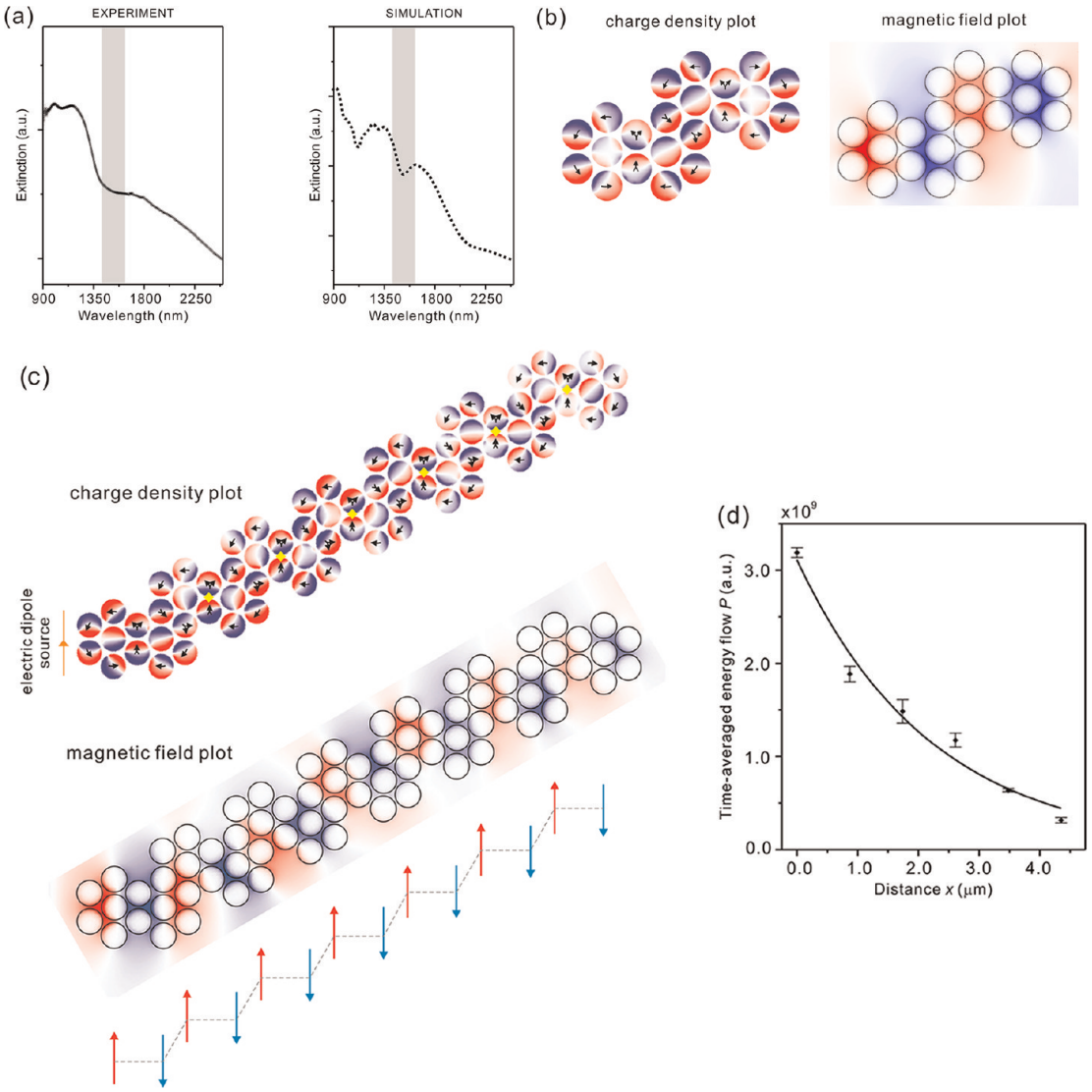

Figure 2. (a) Experimental and simulated extinction spectra of the plasmonic chrysene structure. The magnetic resonance is highlighted by the shaded region around 1500 nm. (b) Simulated charge density and magnetic field plots at 1500 nm. (c) Charge density simulation of a magnetic plasmon steerer with 14 heptamer units along a zigzag chain. An electric dipole source with an amplitude of 1×10^{-9} mA is placed 150 nm in front of the leftmost heptamer. (d) Energy flow as a function of distance from the location of excitation. The energy flow values were taken at the heptamer junctions marked with yellow diamonds in (c). The junctions at the two ends of the chain were excluded in the fitting in order to avoid influence from light scattering. The half-length of each error bar was defined as the difference between a full and a half-mesh calculation. Some error bars are too small to visualize clearly. The fitted energy flow equation is $P = 3.1 \times 10^9 \exp(-x/2.2)$, which corresponds to a field decay length of 2.2 μm.

which each heptamer exhibits a Fano resonance field distribution (not shown). Here the longer wavelength feature at 1500 nm is our primary interest (shaded region in Figure 2a). The simulated charge density plot at this resonance is presented in Figure 2b, which shows ring currents circulating in opposite directions around the four heptamers. Despite the fact that there is an offset in the structure, *i.e.*, two heptamers are twisted with respect to the other two, the gold nanoparticles shared between each neighboring heptamer pair work as a mutual link that couples the ring currents of the individual heptamers. The magnetic nature of this resonance can be identified more explicitly in the magnetic field plot, which shows the excited magnetic dipoles oscillating in antiparallel directions from one heptamer to the next (Figure 2b).

Using this plasmonic analogue of chrysene as a building block, we can construct a plasmon waveguide by extending more heptamer units along the twist direction. As shown in Figure 2c, this leads to a chain with zigzag features, and here, we have included a total of 14 heptamers along the entire chain. In our simulations, we excited the waveguide with an electric dipole source at the left end of the chain. Only the first heptamer is excited by the external source; all other heptamers in the chain become resonant due to the aforementioned coupling between neighboring heptamers. In the charge density plot of the heptamer

chain at this resonance, it is apparent that the ring currents flow successively *via* individual heptamers (Figure 2c). This excitation of antiphase ring currents is facilitated by the mutual links between neighboring heptamers. The resulting magnetic dipoles form an "antiferromagnetic" configuration, in which they are aligned alternatively antiparallel, enabling the propagation of magnetic plasmons along the entire chain. As a result, the energy from the dipole source can be transferred and steered *via* magnetic plasmon propagation along the zigzag chain, with bending features much smaller than the wavelength of light. Such a plasmon steerer could be very useful in applications where the transportation of plasmons requires a subwavelength profile as well as directional guidance.

Due to energy dissipation and light scattering, the electromagnetic field intensity decays continuously with increasing propagation distance, as evident in both the charge density and magnetic field plots. In order to characterize the efficiency of our magnetic plasmon waveguide, the time-averaged energy flow P was calculated along the chain. The energy flow values were obtained at the individual junctions where the neighboring heptamers are joined. To minimize interference effects due to light scattering, the heptamer units near the two ends of the chain were excluded from the calculation.[24] The recorded junction positions are indicated by yellow diamonds in Figure 2c. The exponential fit yields a decay length of 2.2 μm (Figure 2d), which corresponds to 4.4 unit cells. This decay length is slightly smaller than that of a linear heptamer chain (2.65 μm),[15] and the difference can be attributed to the additional losses introduced by the zigzag corners. Nevertheless, this magnetic plasmon steerer shows a much better performance compared to electric plasmon propagation along a linear chain of closely spaced gold nanorods, which has a decay length of only 410 nm.[13] Their operating wavelength was 570 nm with a gold rod length of 90 nm, giving rise to a ratio of 6.3. In our case, the operating wavelength is 1500 nm and the particle size is 260 nm, corresponding approximately to a ratio of 6. Therefore, our magnetic plasmon waveguide and their electric plasmon waveguide are very similar regarding their subwavelength nature. In contrast to the electric plasmon waveguide based on a super-radiant electric mode, which suffers from significant dissipation, the radiation loss of our magnetic plasmon waveguide can be substantially suppressed. This low-loss characteristic results from the subradiant nature of the magnetic ring mode, which is only weakly coupled to light and therefore gives rise to much stronger field confinement for efficient plasmon propagation. Indeed, intrinsic losses in plasmonic nanostructures and inevitable imperfections in experiments can lead to weaker coupling between neighboring heptamer units and therefore shorter propagation distances. To compensate for this, one can incorporate a gain medium such as quantum dots or use chemically prepared metallic nanoparticles, which have much higher quality factors and lower losses than evaporated gold nanostructures.

Next, we investigate the optical properties of the plasmonic triphenylene structure. The experimental and simulated extinction spectra for this structure are shown in Figure 3a. The experimental result is in good agreement with the simulation, but with a weaker response of the subradiant modes. When compared to the plasmonic chrysene structure, the simulated spectrum of the plasmonic triphenylene structure exhibits more complexity, specifically, multiple resonance dips. The resonance dips are approximately at 1100, 1300, 1500, and 1900 nm. In the following, we will again investigate the "antiferromagnetically" coupled resonance, which lies at approximately 1500 nm.

Previously, we demonstrated that the magnetic resonance for a conjugated heptamer maintains approximately the same wavelength for similar structures with different heptamer units.[15] Indeed, for the plasmonic triphenylene structure there is a small resonance dip at 1500 nm, which is highlighted by the shaded region in the simulated spectrum (Figure 3a). This resonance, however, is not clearly observable in the experiment. To provide further insight, the simulated absorption spectrum is also presented in Figure 3a. In this case, the structure is excited using an electric dipole source at the end of the leftmost heptamer. The resonances manifest themselves as absorption peaks in the spectrum. Specifically, the resonance at 1500 nm is more pronounced in the absorption spectrum than in the extinction spectrum. The charge density plot simulated at this resonance (Figure 3b) clearly demonstrates the excitation of alternating antiphase ring currents in the four fused heptamers. In particular, the central heptamer acts as a port, directing the current from the leftmost heptamer to the upper and lower heptamers. The corresponding magnetic field plot in Figure 3b shows that the magnetic dipole moment excited in the central heptamer oscillates in an antiparallel manner relative to the three outer heptamers. Owing to the high structural symmetry, the net electric dipole moment of this magnetic resonance is nearly zero, resulting in a dark mode. Such a dark mode is barely visible in the measurement under plane wave excitation at normal incidence, especially when considering the inhomogeneous broadening due to the variations of particle sizes and shapes over different unit cells in the sample. However, it is straightforward to identify this mode in the simulation when using an electric dipole as excitation source, due to its localized fields. The FTIR analysis was performed to provide more insight into understanding the physics of the magnetic modes. For practical applications of these plasmonic waveguides, a local excitation would be needed so that plasmons can propagate from the

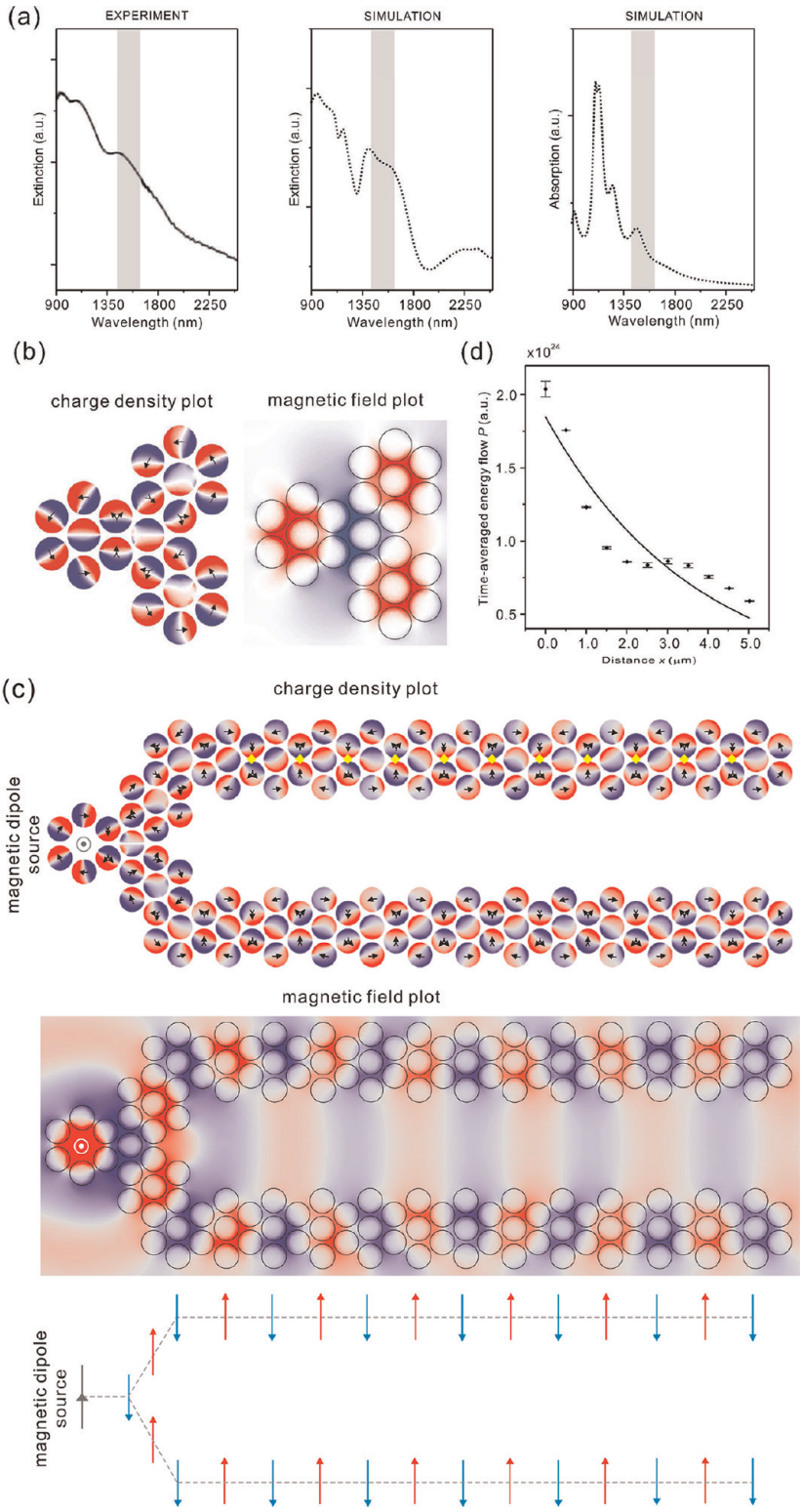

Figure 3. (a) Experimental and simulated extinction spectra of the plasmonic triphenylene structure. The magnetic resonance is highlighted by the shaded region around 1500 nm. (b) Simulated charge density and magnetic field plots at the magnetic resonance. (c) Charge density simulation of a Y-shaped magnetic plasmon splitter with 30 heptamer units. A magnetic dipole source (represented by a concentric circle) with an amplitude of 1×10^{-9} m^2A is placed in the center of the leftmost heptamer by removing its center nanoparticle. (d) Energy flow as a function of distance from the location of excitation. The energy flow values were taken at the heptamer junctions marked with yellow diamonds in (c). The junctions at the two ends of the chain were excluded in order to avoid influence from light scattering. The half-length of each error bar was defined as the difference between a full and a half-mesh calculation. Some error bars are too small to visualize clearly. The fitted energy flow equation is $P = 1.8 \times 10^{24} \exp(-x/3.7)$, corresponding to a field decay length of 3.7 μm.

input end to the output end, performing the role of waveguiding.

We now extend the plasmonic triphenylene structure further by adding hepatamer units along the upper and lower branches. The resulting Y-shaped structure consists of 30 heptamers (Figure 3c). This allows us to examine another interesting excitation scheme, which is unique to magnetic plasmon waveguides. We remove the center particle of the leftmost heptamer in the Y-splitter and place a magnetic dipole source in its center as the excitation source (see Figure 3c). The simulated charge density plot is presented in Figure 3c. The charge density plot clearly demonstrates the formation and propagation of antiferromagnetic-like magnetic plasmons in the waveguide. Ring currents generated from the first heptamer are split at the second heptamer and subsequently flow along the two separate linear heptamer branches. The fully antiparallel arrangement of the excited magnetic dipole moments can be seen clearly in the magnetic field plot in Figure 3c. To quantify the field decay length, we calculated the time-averaged energy flow P at individual junctions along one of the heptamer branches. Due to the intense light scattering and interference effects, the junctions at the two ends of the chain were excluded from this calculation.[24] The recorded junction positions are indicated by the yellow diamonds in the charge density plot in Figure 3c. The analysis reveals a field decay length of 3.7 μm (Figure 3d), corresponding to 7.4 unit cells, which elucidates excellent subwavelength waveguiding performance.

A plasmon Y-splitter can also be used to converge propagating magnetic plasmons from two independent optical paths. In particular, the plasmon propagation can be switched on and off by changing the relative number of the heptamers in the two paths. In Figure 4a, the upper and lower branches contain the same number of heptamers (six in each). In Figure 4b, the upper and lower branches have seven and six heptamers, respectively. In both cases, two in-phase magnetic dipole sources are placed in the centers of the heptamers at the left ends by removing their center nanoparticles. As shown by the simulated magnetic field plot in Figure 4a, when each branch has the same number of heptamers, the magnetic plasmons propagate with the same phase and converge with constructive interference at the center heptamer of the plasmonic triphenylene vertex structure at the right end. The magnetic plasmons then continue to propagate forward, corresponding to an "ON" state. In contrast, when the upper branch has one more heptamer than the lower branch (Figure 4b), the structure yields antiphase magnetic plasmons, which result in destructive interference at the triphenylene structure at the right and no propagation beyond this structure. This situation thus corresponds to an "OFF" state. The "ON" and "OFF" states of the magnetic plasmon propagation

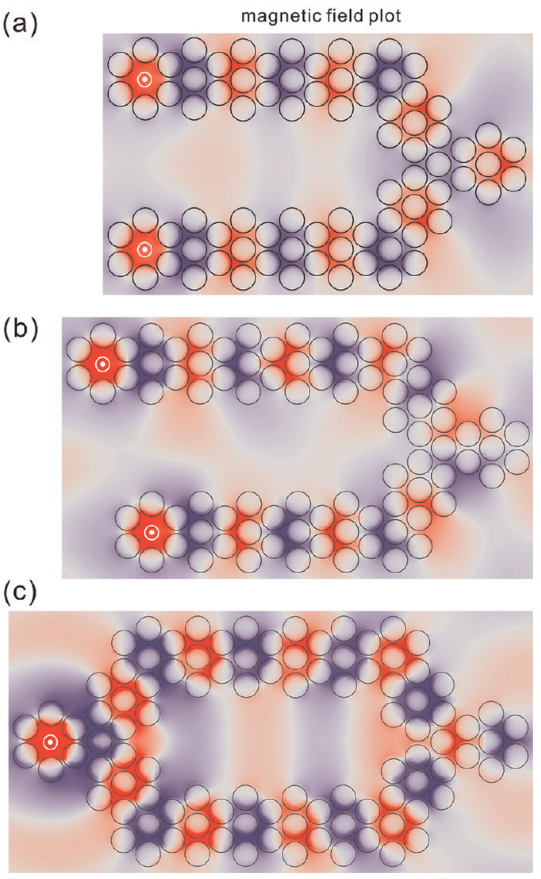

Figure 4. Simulated magnetic field plots of plasmonic Y-splitters for constructive (a) and destructive (b) interference of magnetic plasmons, respectively. In (a), the two branches have an identical number of heptamers. In (b), the upper branch has one more heptamer than the lower branch. (c) Plasmonic Mach–Zehnder interferometer constructed by using two consecutive Y-spliters for splitting and converging magnetic plasmons. The magnetic dipole sources are driven in phase and represented by concentric circles in all cases.

strongly depend on the parity of the heptamer number difference between the two paths. More generally, when the difference between the number of heptamers in each branch is even or odd, the structure is in the "ON" or "OFF" state, respectively. The logic functions of the device can also be altered by changing the relative polarization of the excitation sources.[11] For out-of-phase magnetic dipole excitations, the situation is reversed: for chain lengths differing by an even number of heptamer units, destructive interference at the vertex results in plasmon annihilation and an "OFF" state, while for chain lengths differing by an odd number of heptamer units, constructive interference at the vertex results in further propagation and an "ON" state.

Two consecutive Y-splitters can be used to construct a Mach–Zehnder interferometer, as shown in Figure 4c. The simulated magnetic field plot shows that the magnetic plasmons excited by the magnetic dipole source at the leftmost heptamer propagate through the first triphenylene intersection and subsequently are split

into the two branches. The magnetic plasmons then propagate along the two independent optical paths and converge at the second triphenylene intersection, where constructive interference occurs. The magnetic plasmons then continue to propagate in the forward direction. This entire structure constitutes a plasmonic Mach–Zehnder interferometer, which can be widely applicable for splitting signals in optical circuits.

CONCLUSION

In summary, we have demonstrated magnetic plasmon propagation in metallic nanocluster networks. Our magnetic plasmon waveguides exhibit long propagation lengths, significant subwavelength character, and rich functionalities. We have presented examples of several magnetic plasmon waveguiding devices including a plasmon steerer, a splitter, and a Mach–Zehnder interferometer. The manipulation of magnetic plasmons in heptamer interconnects can further be expanded to more complex systems, for example, by integrating more optical paths to achieve multiple-input and output plasmonic networks.[25] With their compact dimensions, outstanding low-loss propagation characteristics, and range of functionalities, magnetic plasmon-based devices based on these structures should be key to the further development of high-performance energy transport components in information processing and data storage applications.[26]

Conflict of Interest: The authors declare no competing financial interest.

Acknowledgment. We acknowledge Jens Dorfmüller for his material visualizations. N.L. thanks the support of K. Bala Texas Instruments Visiting Professorship in Electrical and Computer Engineering at Rice University. S.M., L.V.B., K.B., Y.L., P.N., and N.J. H. were supported by the Robert A. Welch Foundation (C-1220 and C-1222), the Air Force Office of Scientific Research (FA9550-10-1-0469), the Office of Naval Research (N00014-10-1-0989), the National Science Foundation (IGERT) (DGE-0504425), the DoD NSSEFF (N00244-09-1-0067), and the Defense Threat Reduction Agency (DTRA) (HDTRA1-11-1-0040).

Supporting Information Available: Propagation characteristics of the zigzag structure and robustness of the simulations to small structural defects. This material is available free of charge *via* the Internet at http://pubs.acs.org.

REFERENCES AND NOTES

1. Prodan, E.; Radloff, C.; Halas, N. J.; Nordlander, P. A Hybridization Model for the Plasmon Response of Complex Nanostructures. *Science* **2003**, *302*, 419–422.
2. Lassiter, J. B.; Aizpurua, J.; hernandez, L. I.; Brandl, D. W.; Romero, I.; Lal, S.; Hafner, J. H.; Nordlander, P.; Halas, N. J. Close Encounters between Two Nanoshells. *Nano Lett.* **2008**, *8*, 1212–1218.
3. Liu, N.; Guo, H. C.; Fu, L. W.; Kaiser, S.; Schweizer, H.; Giessen, H. Three-Dimensional Photonic Metamaterials at Optical Frequencies. *Nat. Mater.* **2008**, *7*, 31–37.
4. Liu, N.; Kaiser, S.; Giessen, H. Magnetoinductive and Electroinductive Coupling in Plasmonic Metamaterial Molecules. *Adv. Mater.* **2008**, *20*, 4521–4525.
5. Fan, J. A.; Wu, C. H.; Bao, K.; Bao, J. M.; Bardhan, R.; Halas, N. J.; Manoharan, V. N.; Nordlander, P.; Shvets, G.; Capasso, F. Self-Assembled Plasmonic Nanoparticle Clusters. *Science* **2010**, *328*, 1135–1138.
6. Hentschel, M.; Saliba, M.; Vogelgesang, R.; Giessen, H.; Alivisatos, A. P.; Liu, N. Transition from Isolated to Collective Modes in Plasmonic Oligomers. *Nano Lett.* **2010**, *10*, 2721–2726.
7. Artar, A.; Yanik, A. A.; Altug, H. Multispectral Plasmon Induced Transparency in Coupled Meta-Atoms. *Nano Lett.* **2011**, *11*, 1685–1689.
8. Gallinet, B.; Martin, O. J. F. Influence of Electromagnetic Interactions on the Line Shape of Plasmonic Fano Resonances. *ACS Nano* **2011**, *5*, 8999–9008.
9. Lukyanchuk, B.; Zheludev, N. I.; Maier, S. A.; Halas, N. J.; Nordlander, P.; Giessen, H.; Chong, C. T. The Fano Resonance in Plasmonic Nanostructures and Metamaterials. *Nat. Mater.* **2010**, *9*, 707–715.
10. Bozhevolnyi, S.; Volkov, V. S.; Devaux, E.; Laluet, J. Y.; Ebbesen, T. W. Channel Plasmon Subwavelength Waveguide Components Including Interferometers and Ring Resonators. *Nature* **2006**, *440*, 508–511.
11. Wei, H.; Li, Z. P.; Tian, X. R.; Wang, Z. X.; Cong, F. Z.; Liu, N.; Zhang, S. P.; Nordlander, P.; Halas, N. J.; Xu, H. X. Quantum Dot-Based Local Field Imaging Reveals Plasmon-Based Interferometric Logic in Silver Nanowire Networks. *Nano Lett.* **2011**, *11*, 471–475.
12. Wei, H.; Wang, Z. X.; Tian, X. R.; Kaell, M.; Xu, H. X. Cascaded Logic Gates in Nanophotonic Plasmon Networks. *Nat. Commun.* **2011**, *2*, 387.
13. Maier, S. A.; Kik, P. G.; Atwater, H. A.; Meltzer, S.; Harel, E.; Koel, B. E.; Requicha, A. A. G. Local Detection of Electromagnetic Energy Transport below the Diffraction Limit in Metal Nanoparticle Plasmon Waveguides. *Nat. Mater.* **2003**, *2*, 229–232.
14. Brongersma, M. L.; Hartman, J. W.; Atwater, H. A. Electromagnetic Energy Transfer and Switching in Nanoparticle Chain Arrays Below the Diffraction Limit. *Phys. Rev. B* **2000**, *62*, R16356.
15. Liu, N.; Mukherjee, S.; Bao, K.; Brown, L. V.; Dorfmueller, J.; Nordlander, P.; Halas, N. J. Magnetic Plasmon Formation and Propagation in Artificial Aromatic Molecules. *Nano Lett.* **2012**, *12*, 364–369.
16. Jonathan, C; Greeves, N.; Warren, S.; Wothers, P. In *Organic Chemistry*; Oxford University Press: Oxford, Oxfordshire, 2001.
17. Maier, S. A.; Brongersma, M. L.; Kik, P. G.; Meltzer, S.; Requicha, A. G.; Atwater, H. A. Plasmonics-A Route to Nanoscale Optical Devices. *Adv. Mater.* **2001**, *13*, 1501–1505.
18. Maier, S.; Atwater, H. A. Plasmonics: Localization and Guiding of Electromagnetic Energy in Metal/Dielectric Structures. *J. Appl. Phys.* **2005**, *98*, 011101.
19. Shamonina, E.; Kalinin, V. A.; Ringhofer, K. H.; Solymar, L. Magneto-inductive Waveguide. *Electron. Lett.* **2002**, *38*, 371–373.
20. Liu, N.; Giessen, H. Coupling Effects in Optical Metamaterials. *Angew. Chem., Int. Ed.* **2010**, *49*, 9838–9852.
21. Miroshnichenko, A. E.; Lukyanchuk, B.; Maier, S. A.; Kivshar, Y. S. Optically Induced Interaction of Magnetic Moments in Hybrid Metamaterials. *ACS Nano* **2012**, *6*, 837–842.
22. Liu, H.; Genov, D. A.; Wu, D. M.; Liu, Y. M.; Steele, J. M.; Sun, C.; Zhu, S. N.; Zhang, X. Magnetic Plasmon Propagation Along a Chain of Connected Subwavelength Resonators at Infrared Frequencies. *Phys. Rev. Lett.* **2006**, *97*, 243902.
23. Johnson., P. B.; Christy, R. W. Optical Constants of the Noble Metals. *Phys. Rev. B* **1972**, *6*, 4370–4379.
24. Quinten, M.; Leitner, A.; Krenn, J. R.; Aussenegg, F. R. Electromagnetic Energy Transport *via* Linear Chains of Silver Nanoparticles. *Opt. Lett.* **1998**, *23*, 1331–1333.
25. Dregely, D.; Hentschel, M.; Giessen, H. Excitation and Tuning of Higher-Order Fano Resonances in Plasmonic Oligomer Clusters. *ACS Nano* **2011**, *5*, 8202–8211.
26. Engheta, N. Circuits with Light at Nanoscales: Optical Nanocircuits Inspired by Metamaterials. *Science* **2007**, *317*, 1689–1702.